Biomechan Model Mechanobiol (2005) 4: 57–61
DOI 10.1007/s10237-004-0059-2

SHORT COMMUNICATION

T. I. Zohdi

A simple model for shear stress mediated lumen reduction in blood vessels

Received: 10 October 2004 / Accepted: 2 December 2004 / Published online: 13 May 2005

Abstract The goal of this paper is to qualitatively describe the dominant flow characteristics associated with shear stress mediated lumen reduction due to atherosclerotic plaque growth. The approach is to develop rate equations for the reduction of the lumen as a function of the shear stress near the intima wall. Elementary, qualitative, models for fully developed laminar and turbulent flows are employed, leading to nonlinear ordinary differential equations. The model provides a qualitative description of one aspect of the long-term reduction, perhaps taking years, of the lumen due to wall growth. This is useful because of the extreme complexity of long-term experiments.

Keywords Lumen reduction · Atherosclerotic plaque growth

1 Introduction

The primary goal of this paper is to qualitatively describe the dominant flow characteristics associated with shear stress mediated lumen reduction in blood vessels due to atherosclerotic plaque growth. In such cases, lumen reduction is frequently attributed to microscale suspensions, which adhere to, and penetrate, the intima wall. Specifically, the growth of atherosclerotic plaque is believed to be initiated by the presence and oxidation of excess low-density lipoprotein (LDL) in the intima. Stages in that process appear to be (a) adhesion of monocytes to the endothelial surface, which is controlled by the adhesion molecules stimulated by the excess LDL, the oxygen content, and the intensity of the blood flow; (b) penetration of the monocytes into the intima and subsequent inflammation of the tissue; and (c) rupture of the plaque accompanied by some degree of thrombus formation or even subsequent occlusive thrombosis. Plaques with high risk of rupture are termed *vulnerable*, (see, for Fuster 2002). Currently, no adequate, robust, diagnostic strategy for the identification of vulnerable plaques is available. Surveys of the current thinking in the medical community pertaining to the growth and rupture of atherosclerotic plaques are provided in Shah (1997), van der Wal and Becker (1999), Chyu and Shah (2001), Libby (2001a, b) Richardson et al. (1989), Loree et al. (1992), Davies et al. (1993), among others. For numerical and theoretical fluid flow analyses we refer the reader to Stroud et al. (2000, 2002), Berger and Jou (2000) and Jou and Berger (1998). For experimental-oriented physiological flow studies of atherosclerotic carotid bifurcations and related systems, see Bale-Glickman et al. (2003a, b). Notably, Bale-Glickman et al. (2003a, b) have developed flow models which replicate the lumen of plaques excised intact from patients with severe atherosclerosis, which have shown that the complex internal geometry of the diseased artery, combined with the pulsatile input flows, gives exceedingly complex flow patterns. They have shown that the flows are highly three dimensional and chaotic, with details varying from cycle to cycle. In particular, the vorticity and streamline maps confirm the highly complex and three-dimensional nature of the flow. In the realm of mechanobiology, extensive stress analyses in healthy and diseased arteries have been investigated in the works Holzapfel and co-workers (Holzapfel et al. 2000, 2002a, 2002b; and Holzapfel and Ogden 2003). Overviews focusing on various types of soft biotissue can be found in Humphrey (2002) among others. The mechanisms involved in the initial stages of of the disease, in particular stage (a), have not been extensively studied, although some preliminary studies have been carried out recently in Zohdi et al. (2003).

Regardless of the exact mechanism of effective growth, it appears to be correlated to the presence of suspensions near the intima wall. This is primarily controlled by the intensity of the shear stress near the wall. High shear stresses tend to impede microscale suspensions from adhering to the intima, while low shear

T. I. Zohdi
Department of Mechanical Engineering,
University of California, Berkeley, CA 94720-1740, USA

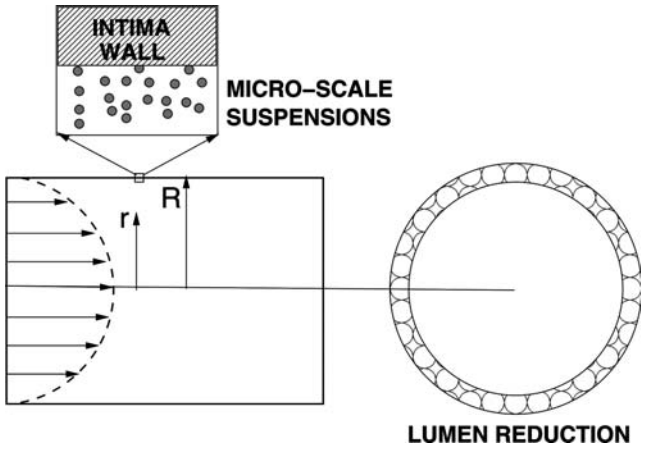

Fig. 1 Flow through the lumen with wall growth

stresses allow the suspensions to adhere to the wall. The purpose of this study is to investigate the dependency of shear-controlled growth on flow parameters, such as the velocity profile, flow rate, etc. The approach is to develop rate equations for the reduction of the lumen as a function of the shear stress near the intima wall. Elementary, qualitative, models for fully developed laminar and turbulent flows are employed, leading to nonlinear ordinary differential equations which govern the reduction of the lumen over time.

2 Elementary qualitative models

We start by developing a simple model to describe how the circular cross section of an idealized lumen, $A = \pi R^2$ (Fig. 1), changes due to microscale deposits building up onto its surface. The inner radius of the lumen, which changes over time, is denoted by R. The initial cross-sectional area is $A_0 = \pi R_0^2$. We consider simple fully developed (incompressible) flow profiles, with constant overall flow rate ($Q_0 = v_0 A_0 = \int_A v \, dA = Q$), through the lumen, given by ($q \geq 2$)[1]

$$v = v_{\max}\left(1 - \left(\frac{r}{R}\right)^q\right), \tag{1}$$

where, in a phenomenological sense, as q increases, one characterizes, qualitatively, progressively turbulent flow. The corresponding shear stress is given by

$$\tau = \mu \frac{\partial v}{\partial r}. \tag{2}$$

Because the overall flow rate is assumed constant ($Q_0 = Q$), one has

$$v_{\max} = \frac{Q_0(q+2)}{Aq}. \tag{3}$$

[1]For fully developed laminar flow, $q = 2$.

Therefore, shear stress near the wall, specifically at $r = kR$, $0 \leq k \leq 1$, is given by

$$\tau_{\mathrm{nw}} = \mu \left.\frac{\partial v}{\partial r}\right|_{r=kR} = -\mu \frac{Q_o(q+2)}{\pi R^3} k^{q-1}. \tag{4}$$

Phenomenologically speaking, the ability of a microscale suspension to adhere to the intima wall is controlled by the intensity of the shear stress near the wall. Higher shear stresses reduce the likelihood of microscale suspensions adhering to the intima wall, while lower shear stresses allow the suspensions to adhere to the wall. Accordingly, consider a growth law where the rate of growth is proportional to the ratio of shear stress near the wall to a critical "detachment" stress $|\tau_{\mathrm{nw}}| \leq \tau^*$

$$\begin{aligned} \dot{R} &= -\eta \max\left(0, 1 - \frac{|\tau_{\mathrm{nw}}|}{\tau^*}\right) \\ &= -\eta \max\left(0, 1 - \frac{\mu Q_o (q+2) k^{q-1}}{\tau^* \pi R^3}\right), \end{aligned} \tag{5}$$

where η is a growth rate constant. As the velocity increases, suspensions are less likely to adhere. Thus, for increasing q (progressively tending toward turbulent behavior), there will be less growth (less reduction in R). Thus, we have no growth if

$$|\tau_{\mathrm{nw}}| = \mu \frac{Q_o(q+2)k^{q-1}}{\pi R^3} \geq \tau^*. \tag{6}$$

The steady state value of R can be determined by setting $\dot{R} = 0$, leaving

$$R(t=\infty) = \left(\frac{\mu Q_o (q+2) k^{q-1}}{\tau^* \pi}\right)^{1/3}. \tag{7}$$

The obvious steady state trends are:

- An increase in τ^* leads to more growth (reduction of R)
- An increase in Q_o leads to less growth
- An increase in μ leads to less growth.

The dependence of the behavior of R on q (governing the flow profile) is somewhat less obvious, due to the product of "competing" terms involving q, in Eq. 7. Taking the partial derivative of R with respect to q yields, at $t = \infty$,

$$\frac{\partial R}{\partial q} = \frac{R}{3}\left(\frac{1}{q+2} + \ln k\right). \tag{8}$$

Now setting the derivative to zero, and solving for q yields

$$q = \frac{1}{\ln k} - 2 \stackrel{\mathrm{def}}{=} q^*, \tag{9}$$

or

$$k = \mathrm{e}^{-\frac{1}{q^*+2}}. \tag{10}$$

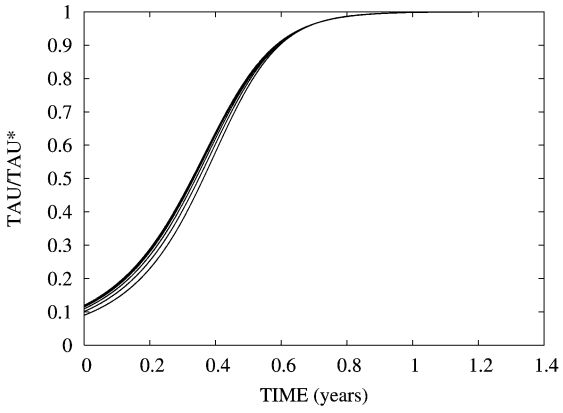

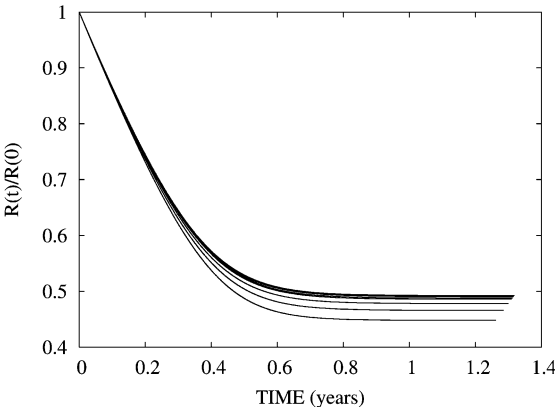

Fig. 2 The behavior of the shear stress ratio at $r = kR = 0.9R$ and the growth (reduction of the lumen radius) for $q = 2, 3, 4, 5, 6, 7, 8, 9$, and 10. The *top curve* (forming an upper envelope) corresponds to $q = 7$, which is closest to the maximizer, $q^* = 7.49$

Since $\ln k \leq 0$ for $0 \leq k \leq 1$ and the range of admissible q is $2 \leq q$, there is the possibility that q^* could be a maximizer or minimizer of R. Clearly, since

$$\frac{\partial^2 R}{\partial q^2} = \frac{\partial R}{\partial q}\frac{1}{3}\left(\frac{1}{q+2} + \frac{\ln k}{3}\right) + \frac{R}{3}\left(-\frac{1}{(q+2)^2}\right), \tag{11}$$

and setting $\partial R/\partial q = 0$, for $q = q^*$, we have

$$\left.\frac{\partial^2 R}{\partial q^2}\right|_{q=q^*} = \frac{R}{3}\left(\frac{1}{(q^*+2)^2}\right) < 0, \tag{12}$$

which indicates that, at $q = q^*$, R is maximized. In other words, if $q = q^*$, the least amount of growth occurs. It is interesting to note that the radius is maximized by a specific finite value of $q = q^*$, and for higher q values, the radius again decreases. Clearly, the lower limit of achievable q^* is $q^* = 2$ (laminar flow), leading to a corresponding value of $k = e^{-\frac{1}{4}}$, while as $k \to 1$, $q^* \to \infty$, which indicates that a more blunted ("turbulent") flow profile would be optimal if a smaller critical distance away from the wall were chosen. The maximum steady state value that the radius can attain ($R(t = \infty)$) can be ascertained by inserting Eq. 9 into Eq. 7, to obtain

$$R(t = \infty)|_{q=q^*} = \left(-\frac{\mu Q_o}{\tau^* \pi e k^3 \ln k}\right)^{1/3}, \tag{13}$$

which provides a relationship between the minimum wall growth and the critical wall distance parameter.

In order to illustrate the time-dependent behavior of the model, consider the following nominal parameters:

- $R(t = 0) = 0.001$ m
- $v(t = 0) = 0.1$ m/s,
- $\eta = -10^{-10}$ m/s
- $\mu = 0.0005$ Pa/s
- $\tau^* = 1$ Pa.

For the parameters chosen, $q^* = 7.49$ is the maximizer of R. Figure 1 depicts the results when these parameters are employed. The simulations were carried out with a simple forward Euler time integration of the form:

$$R(t + \Delta t) = R(t) + \Delta t \mathcal{F}(R(t)), \tag{14}$$

where $\mathcal{F}(R) = -\eta \max(0, 1 - (|\tau_{nw}|/\tau^*))$. As indicated in Fig. 1, eventually, the growth slows, then terminates[2], once the lumen narrows sufficiently to raise the fluid-induced shear stress to exceed the threshold value of τ^*.

Remark 1: One can define a nondimensional number which indicates whether wall growth will begin, by taking the ratio of the initial shear stress ($t = 0$) to the critical shear stress

$$\mathcal{G} \stackrel{\text{def}}{=} \mu \frac{Q_o(q+2)k^{q-1}}{\tau^* \pi R^3(t=0)}. \tag{15}$$

If $\mathcal{G} \geq 1$, then no growth occurs, while if $\mathcal{G} < 1$, then growth begins.

Remark 2: We remark that in a more general setting, not necessarily associated with plaque, or even biological processes, for example corrosion processes and oxide film growth (Fontana 1986), the flow-induced reduction of the lumen of channels is attributed to film build up onto the surface of a wall. Essentially, the same modeling approach could be followed to qualitatively describe those scenarios as well.

3 Concluding remarks and extensions

The model provides a qualitative description of one aspect of the long-term reduction, perhaps taking years, of the lumen due to wall growth. This is useful because of the extreme complexity of long-term experiments. An interesting observation is that the velocity profile that maximizes the radius (minimizes the growth) is a specific finite value of $q = q^*$, and for higher q values, the radius again decreases. However, as the radius of the lumen changes, the type of flow profile will change; in other

[2] A time step of 1 h, $\Delta t = 3600$ s, which was extremely small (an "overkill") relative to the overall simulation time scale of 1 year, was used in this explicit time-marching method. An explicit time-marching scheme was perfectly adequate for this relatively simple single degree of freedom system.

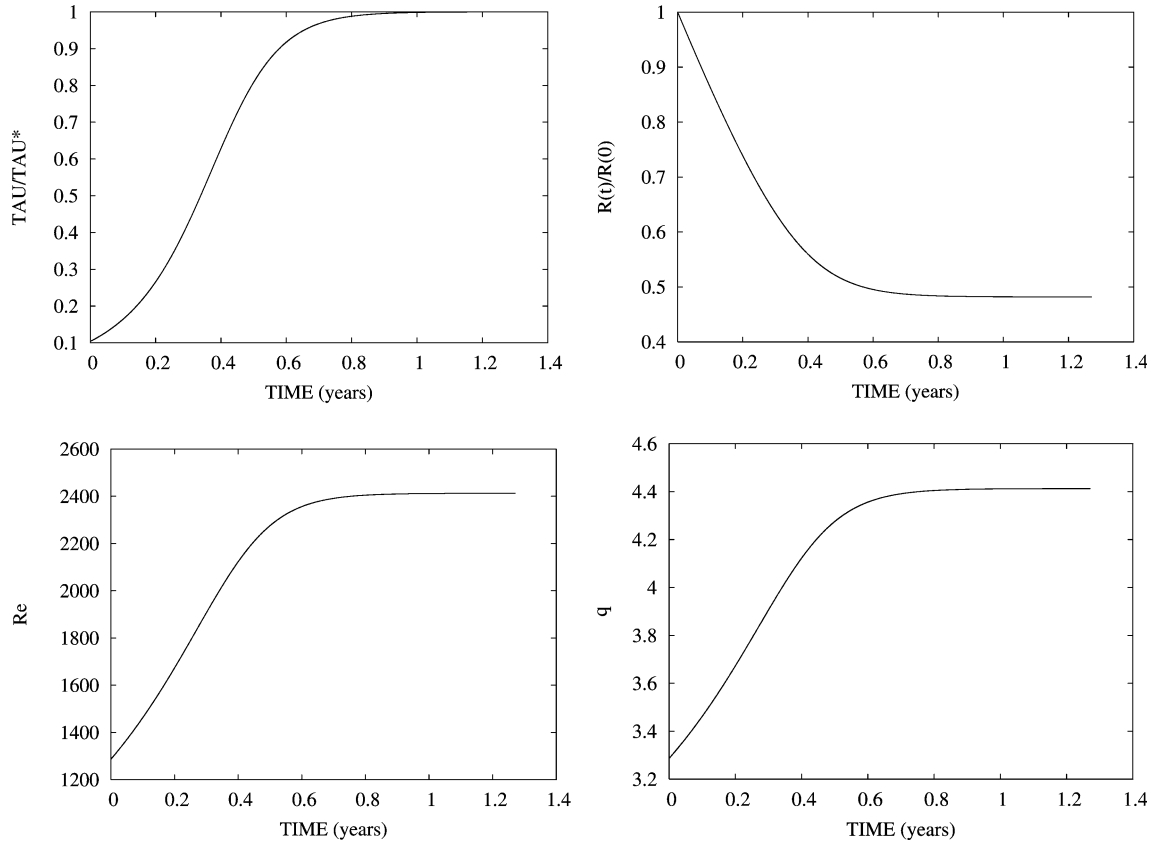

Fig. 3 The behavior of the shear stress, growth (reduction of the lumen radius), centerline Reynolds' number, and velocity profile over time for $kR = 0.9R$, $q = c_1 \mathrm{Re}_c + c_2$

words, q is not fixed. This was not reflected in the previous model; in other words, the flow profile and growth are not fully coupled. In order to capture the effect of a changing profile, we represent q as a linear function of the centerline Reynolds' number, $\mathrm{Re}_c = \rho v_{\max} 2R/\mu$

$$q = q(R) = c_1 Re_c + c_2, \tag{16}$$

where c_1 and c_2 are experimentally determined constants. Well-known models having linear dependency of flow-profile exponents on the Reynolds' number can be found in, for example, Hinze (1975). Typically, $0 \leq c_1 < < 1$ and $c_2 \approx 2$, and, in particular, for laminar flow $c_1 = 0$ and $c_2 = 2$. Since $v_{\max} = Q_0(q+2)/\pi R^2 q$, from Eq. 16 we obtain a quadratic relationship for q,

$$q^2 - (\gamma + c_2)q - 2\gamma = 0, \tag{17}$$

where $\gamma = 2c_1 Q_0 \rho / \pi R \mu$. Solving for q we obtain:[3]

$$q(R) = \frac{1}{2}\left((\gamma + c_2) \pm \sqrt{(\gamma + c_2)^2 + 8\gamma}\right). \tag{18}$$

As before, the shear stress near the wall is given by $\tau_{\mathrm{nw}} = \mu \frac{\partial v}{\partial r}|_{r=kR}$. Now consider the same growth law as before, $\dot{R} = \mathcal{F}(R)$, which is solved using a forward Euler time marching: $R(t + \Delta t) = R(t) + \Delta t \mathcal{F}(R(t))$. The following parameters, in addition to the values introduced earlier, were used: (1) $\rho = 10^3\ kg/m^3$, (2) $c_1 = 10^{-2}$, and (3) $c_2 = 2$. The plots in Fig. 3 depict the results. As one would expect, eventually, the growth slows, once the lumen narrows sufficiently to raise the fluid-induced shear stress to exceed the threshold value of τ^*. As the lumen narrows, the flow becomes relatively more turbulent, i.e. the Reynolds' number increases as does the exponent q, leading to a more blunted profile. We remark that the usual Reynolds' number associated with the onset of turbulent flow is approximately $\mathrm{Re}_c = 2{,}300$, which corresponds quite nicely with the results in Fig. 3, i. e. the wall growth stops when the flow is mildly turbulent.[4]

One should consider either of the previous models as a qualitative a- priori analysis leading, ultimately, toward computationally-intensive large-scale simulations. For example, the following general coupled processes: (a) fluid mechanics, involving the concentration of suspensions, which are nominally convected with the fluid, (b) fluid–solid interaction at the intima wall/fluid interface, leading to penetration or absorption of suspensions into the intima, and (c) growth of the intima wall and an

[3] The larger of the two roots is taken later in the simulations.

[4] The steady state value of R can be determined by setting $\dot{R} = 0$, leaving a formally similar Eq. as 7,

$$R(t = \infty) = \left(\frac{\mu Q_o (q(R) + 2) k^{q(R)-1}}{\tau^* \pi}\right)^{1/3}, \tag{19}$$

where, however, q is a function of R.

accompanying buildup of stress and/or possible damage. As an example consider an abstract form of

$$\Pi_1(c,v,\sigma)=0 \quad (\text{MASS BALANCE}),$$
$$\Pi_2(c,v,\sigma)=0 \quad (\text{FLUID FLOW}),$$
$$\Pi_3(c,v,\sigma)=0 \quad (\text{GROWTH/WALL DEFORMATION}), \tag{20}$$

where c is the concentration of suspensions, v is the fluid velocity field, and σ is the mechanical stress field in the solid. Generally, such schemes proceed, within a discretized time step, by solving each field equation individually, allowing only the corresponding primary field variable (c, v or σ) to be active. This effectively decouples the system of differential equations. After the solution of each field equation, the primary field variable is updated, and the next field equation is solved in a similar manner, with only the corresponding primary variable being active. For accurate numerical solutions, the approach requires small time steps, primarily because the staggering error accumulates with each passing increment. Thus, such computations are usually computationally intensive. For details, see, for example, Zohdi (2002, 2004a, 2004b).

Acknowledgements The author wishes to thank the anonymous reviewers for their constructive criticisms and suggestions, which improved the manuscript.

References

Bale-Glickman J, Selby K, Saloner D, Savas O (2003a) Experimental flow studies in exact-replica phantoms of atherosclerotic carotid bifurcations under steady Input conditions. J Biomech Eng 125:38–48

Bale-Glickman J, Selby K, Saloner D, Savas O (2003b) Physiological flow studies in exact-replica atherosclerotic carotid bifurcation. In: Proceedings of IMECE'03 2003 ASME international mechanical engineering congress and esposition. Washington, pp 16–21

Berger SA, Jou LD (2000) Flow in stenotic vessels. Annu Rev Fluid Mech 32:347–382

Chyu KY, Shah PK (2001) The role of inflammation in plaque disruption and thrombosis. Rev Cardiovas Med 2:82–91

Davies MJ, Richardson PD, Woolf N, Katz DR, Mann J (1993) Risk of thrombosis in human atherosclerotic plaques: role of extracellular lipid, macrophage, and smooth muscle cell content. Br Heart J 69:377–381

Fontana M (1986) Corrosion engineering. McGraw-Hill, New York

Fuster V (ed) (2002) Assessing and modifying the vulnerable atherosclerotic plaque. Futura publishing company, Armonk

Hinze JO (1975) Turbulence. McGraw-Hill, New York

Holzapfel GA, Ogden RW (eds) (2003) Biomechanics of soft tissue in cardiovascular Systems. Springer, Wien

Holzapfel GA, Gasser TC, Ogden RW (2000) A new constitutive framework for arterial wall mechanics and a comparative study of material models. J Elasticity 61:1–48

Holzapfel GA, Gasser TC, Stadler M (2002a) A structural model for the viscoelastic behavior of arterial walls: Continuum formulation and finite element analysis. Eur J Mech A Solids 21:441–463

Holzapfel GA, Stadler M, Schulze-Bauer CAJ (2002b) A layer-specific three-dimensional model for the simulation of balloon angioplasty using Magnetic Resonance imaging and mechanical testing. Ann Biomed Engr 30:753–767

Humphrey JD (2002) Cardiovascular solid mechanics. cells, tissues, and organs. Springer, New York

Jou LD, Berger SA (1998) Numerical simulation of the flow in the carotid bifurcation. Theor Comput Fluid Mech 10:239–248

Libby P (2001a) Current Concepts of the Pathogenesis of the Acute Coronary Syndromes. Circ 104:365–372

Libby P (2001b) The vascular biology of atherosclerosis. In: Braunwald E, Zipes DP, Libby P (eds) Heart diseases. A textbook of cardiovascular medicine, chap 30, sixth edn. Saunders Company, Philadelphia, pp 995–1009

Loree HM, Kamm RD, Stringfellow RG, Lee RT (1992) Effects of Fibrous Cap Thickness on Peak Circumferential Stress in Model Atherosclerotic Vessels. Circ Res 71:850–858

Richardson PD, Davies MJ, Born GVR (1989) Influence of plaque configuration and stress distribution on fissuring of coronary atherosclerotic plaques. Lancet 2(8669):941–944

Shah PK (1997) Plaque disruption and coronary thrombosis: New insight into pathogenesis and prevention. Clin Cardiol 20(Suppl II):38–44

Stroud JS, Berger SA, Saloner D (2000) Influence of stenosis morphology on flow through severly stenotic vessels: implications of plaque rupture. J Biomech 33:443–455

Stroud JS, Berger SA, Saloner D (2002) Numerical analysis of flow through a severly stenotic carotid artery bifurcation. J Biomed Eng 124(1):9–21

van der Wal AC, Becker AE (1999) Atherosclerotic plaque rupture—pathologic basis of plaque stability and instability. Cardiovasc Res 41:334–344

Zohdi TI (2002) An adaptive-recursive staggering strategy for simulating multifield coupled processes in microheterogeneous solids. Int J Num Methods Engr 53:1511–1532

Zohdi TI (2004a) A computational framework for agglomeration in thermo-chemically reacting granular flows. Proc R Soc 460:3421–3445

Zohdi TI (2004b) Modeling and simulation of a class of coupled thermo-chemo-mechanicalprocesses in multiphase solids. Comput Methods Appl Mech Eng 193(6-8):679–699

Zohdi TI, Holzapfel GA, Berger SA (2003) A phenomenological model for atherosclerotic plaque growth and rupture. J Theor Biol 227:437–443